

Wavefront singularities associated with the conical point in elastic solids with cubic symmetry

Andrew N. Norris

*Rutgers University, Department of Mechanical and Aerospace Engineering, 98
Brett Road, Piscataway, NJ 08854, norris@rutgers.edu*

Abstract

The wavefronts from a point source in a solid with cubic symmetry are examined with particular attention paid to the contribution from the conical points of the slowness surface. An asymptotic solution is developed that is uniform across the edge of the cone in real space, the interior of which contains the plane lid wavefront analyzed by Burridge [6]. The uniform solution also contains the regular wavefronts away from the cone edge, a delta pulse on one side and its Hilbert transform on the other. In the direction of the cone edge the three wavefronts merge to produce a singularity of the form $H(t)t^{-3/4}$.

1 Introduction

We consider the time dependent Green's function in solids of cubic symmetry, with focus on the field across the "flat lid" associated with the conical degeneracy. Such conical points occur in the [111] directions in every material displaying cubic symmetry [12]. It is well known that the Green's function in anisotropic crystals can be split into a continuous field and a sequence of singularities. The latter are associated with *regular* points on the slowness surface with outward normal in the direction of the observer. Burridge [6] provided explicit expressions for the field contributions from regular points, whether they occur on sections of the slowness surface that are locally convex, concave or saddle shaped. He also derived the peculiar singular behavior on the flat lids of the wave surface associated with the conical points. The singularity on the flat lid is a step function in time, in contrast to the more singular delta pulse or its Hilbert transform (a $1/t$ pulse) which arise from regular points on the slowness surface. Furthermore, the wavefront on the flat lid decays with distance like $1/r^2$, in contrast to the $1/r$ decay from regular points. The analysis in [6] was limited to receiver positions inside the lid but not too close to the lid edge. Here we develop solutions that include Burridge's flat lid solution, but also display the transition across the lid edge. In particular a uniform solution is derived that incorporates the regular and the flat lid wavefronts.

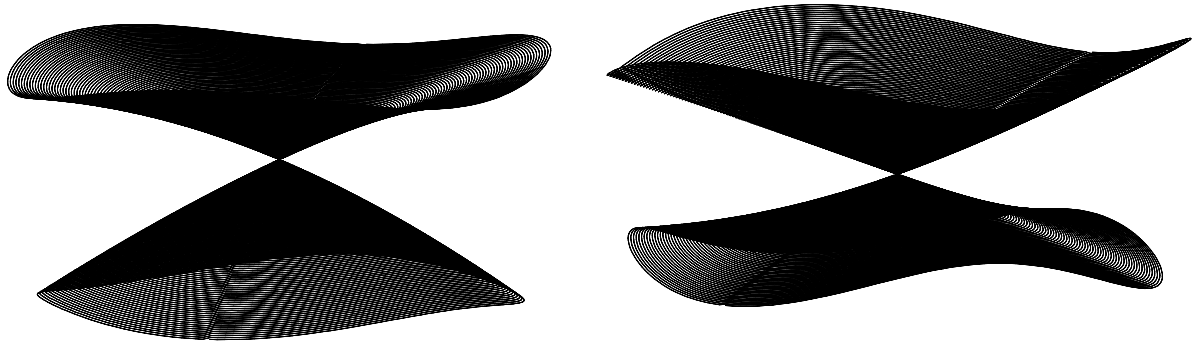


Fig. 1. The neighborhood of a conical point on the slowness surface for iron (left) and potassium chloride (right). The two quasi-transverse sheets are shown for a sector of 7° angular extent about the 111-axis (defined such that $|\xi_\phi/\xi_3| < \tan 7^\circ$ in the notation of eq. (11)).

Several studies of the elastic wavefield from conical points appeared after the original work of Burridge [6]. Barry and Musgrave [4] reduced the solution arising from elliptical conical points in tetragonal media to a single integral requiring numerical quadrature. Payton [13] considered the effects of double points in the slowness surface of a special type of transversely isotropic solid with the restriction $c_{11} = c_{33} = c_{23}$. This exhibits conical points on the symmetry axis as well as a ring of double points in the plane perpendicular to the axis. Based on the material restriction he was able to construct explicit integral solutions for a point force in the form of elliptic integrals which show that the wave front of conical points have lids, while the circular double points do not produce lids. Borovikov [5] is the only work that has considered a uniform solution valid across the edge of the flat lid. Borovikov's solution is, however, time harmonic and not directly applicable to the problem considered here, which we find more easily addressed by a suitable modification of Burridge's original approach.

The purpose of this paper is to examine the way in which the singularity from the conical point, i.e., the flat lid wavefront, coalesces with the nearby regular wavefronts at their common meeting points along the directions of the conical boundary in real space. First we review some of the necessary preliminary results from [6] and examine the topology of the neighborhood of a conical point. The major results follow from the use of a locally parabolic approximation near the conical point, which allows certain closed form solutions of the Green's function. In particular, we derive a uniform approximation that includes the regular wavefronts and the flat lid singularity, and is uniform across the edge of the lid in real space. The solution also generates the singular form of the Green's function in the direction of the lid edge.

The outline of the paper is as follows. The general theory for the Green's function in

anisotropic solids is reviewed in section 2. Materials with cubic symmetry are considered in section 3 where the conical point is defined. The local behavior of the slowness and wave surfaces is discussed in section 3, and the crucial slowness surface curvature is introduced. The Green's function is reduced to a single integral in section 4 and the dominant contributions to the wave field are derived. This includes the flat lid response and the regular wavefronts associated with the direct waves. Section 5 provides a uniform description appropriate to the conical point, using a generic function which incorporates the flat lid singularity and the regular wavefront singularities.

2 General theory for anisotropic solids

We are concerned with the fundamental solution, $\mathbf{G}(\mathbf{x}, t)$ with elements G_{ij} , which solves

$$\rho \partial_t^2 G_{im}(\mathbf{x}, t) - C_{ijkl} \partial_j \partial_l G_{km}(\mathbf{x}, t) = \rho \delta_{im} \delta(t) \delta(\mathbf{x}), \quad (1a)$$

$$G_{ij}(\mathbf{x}, t) = 0, \quad t < 0. \quad (1b)$$

Here $\delta(t)$ is the Dirac delta and $\delta(\mathbf{x}) = \delta(x_1)\delta(x_2)\delta(x_3)$, where the subscripts (the summation convention is understood) i, j, \dots take on the values 1, 2 and 3 and refer to a rectangular coordinate system. The elastic moduli satisfy the symmetries $C_{ijkl} = C_{jikl}$, $C_{ijkl} = C_{klji}$, and are positive definite, $C_{ijkl} a_{ij} a_{kl} > 0$ for all symmetric non-zero \mathbf{a} . Although there are now several alternative ways to express $\mathbf{G}(\mathbf{x}, t)$, e.g. [10], we use the succinct Herglotz-Petrowski formula [7] derived by Burridge [6],

$$\mathbf{G}(\mathbf{x}, t) = \int_S dS \mathbf{F}(\boldsymbol{\xi}) \delta'(t - \boldsymbol{\xi} \cdot \mathbf{x}), \quad (2a)$$

$$\mathbf{F}(\boldsymbol{\xi}) = -\frac{1}{8\pi^2} \frac{\mathbf{A}(\boldsymbol{\xi}) \mathbf{A}^T(\boldsymbol{\xi})}{|\nabla v(\boldsymbol{\xi})|}, \quad \boldsymbol{\xi} \in S. \quad (2b)$$

Here, S is the entire slowness surface; $\boldsymbol{\xi}$ is the slowness vector on S ; $\mathbf{A}(\boldsymbol{\xi})$ is the associated unit polarization vector; the phase speed function $v(\boldsymbol{\xi})$ is a homogeneous function of degree one in $\boldsymbol{\xi}$, and they are related by

$$Q_{ik}(\hat{\boldsymbol{\xi}}) A_k(\boldsymbol{\xi}) = \rho v^2(\hat{\boldsymbol{\xi}}) A_i(\boldsymbol{\xi}), \quad (3)$$

where

$$Q_{ik}(\hat{\boldsymbol{\xi}}) = C_{ijkl} \hat{\xi}_j \hat{\xi}_l, \quad \text{and} \quad \hat{\boldsymbol{\xi}} = \boldsymbol{\xi}/\xi. \quad (4)$$

The eigenvalue equation (3) admits of three roots for v^2 , corresponding to the three sheets of the slowness surface. The integral (2a) is therefore over the union of the three sheets. Note that $v(\boldsymbol{\xi}) = 1$ on S , implying that the physical (dimensional) phase speed is $v(\hat{\boldsymbol{\xi}}) = 1/\xi$. Another property that follows from the functional form of v as a homogeneous function of its argument is that the gradient appearing in eq. (2b) is the wave (or group) velocity: $\mathbf{c} = \nabla v(\boldsymbol{\xi})$.

3 Conical points of the cubic slowness surface

3.1 Elastic moduli for cubic symmetry

We use a slightly different notation than that of Burridge [6], with the purpose of obtaining a higher order approximation to the slowness surface in the vicinity of the conical point. The elastic stiffness is

$$\mathbb{C} = 3\lambda \mathbb{J} + 2\mu_1 \mathbb{I} + 2(\mu_2 - \mu_1) \mathbb{D}, \quad (5)$$

where the tensors are as follows: $\mathbb{I}\mathbf{S} = \mathbf{S}$, $\mathbb{J}\mathbf{S} = \frac{1}{3}(\text{tr } \mathbf{S})\mathbb{I}$ for all $\mathbf{S} \in \text{Sym}$, and \mathbb{D} is a fourth order tensor defined by the cube axes $\{\mathbf{a}, \mathbf{b}, \mathbf{c}\}$, as

$$\mathbb{D} = \mathbf{a} \otimes \mathbf{a} \otimes \mathbf{a} \otimes \mathbf{a} + \mathbf{b} \otimes \mathbf{b} \otimes \mathbf{b} \otimes \mathbf{b} + \mathbf{c} \otimes \mathbf{c} \otimes \mathbf{c} \otimes \mathbf{c}. \quad (6)$$

The stiffness is positive definite if and only if $\mu_1 > 0$, $\mu_2 > 0$ and $\lambda + \frac{2}{3}\mu_2 > 0$. The non-zero elastic moduli in the Voigt notation are $c_{11} = c_{22} = c_{33} = \lambda + 2\mu_2$, $c_{12} = c_{23} = c_{31} = \lambda$ and $c_{44} = c_{55} = c_{66} = \mu_1$.

The eight conical points on S occur symmetrically in each octant, although we restrict our attention to the conical point in the $(+++)$ octant. Two illustrations of sections of S through the conical point can be found in Figures 2 and 3. In order to examine the local behavior of S we introduce the new basis set of vectors

$$\mathbf{e}_1 = \frac{1}{\sqrt{6}}(-1, -1, 2), \quad \mathbf{e}_2 = \frac{1}{\sqrt{2}}(1, -1, 0), \quad \mathbf{e}_3 = \frac{1}{\sqrt{3}}(1, 1, 1). \quad (7)$$

When referred to these axes the moduli become, using a slight modification of eq. (3.46) in [3],

$$\mathbf{c}' = \begin{bmatrix} c'_{11} & c'_{12} & c'_{13} & 0 & -c'_{46} & 0 \\ c'_{12} & c'_{11} & c'_{13} & 0 & c'_{46} & 0 \\ c'_{13} & c'_{13} & c'_{33} & 0 & 0 & 0 \\ 0 & 0 & 0 & c'_{44} & 0 & c'_{46} \\ -c'_{46} & c'_{46} & 0 & 0 & c'_{44} & 0 \\ 0 & 0 & 0 & c'_{46} & 0 & c'_{66} \end{bmatrix}, \quad (8)$$

where

$$\begin{aligned} c'_{11} &= \lambda + 2\mu_2 - (\mu_2 - \mu_1), & c'_{33} &= \lambda + 2\mu_2 - \frac{4}{3}(\mu_2 - \mu_1), \\ c'_{12} &= \lambda + \frac{1}{3}(\mu_2 - \mu_1), & c'_{13} &= \lambda + \frac{2}{3}(\mu_2 - \mu_1), \\ c'_{44} &= \mu_2 - \frac{1}{3}(\mu_2 - \mu_1), & c'_{66} &= \mu_2 - \frac{2}{3}(\mu_2 - \mu_1), \\ c'_{46} &= \frac{\sqrt{2}}{3}(\mu_2 - \mu_1). \end{aligned}$$

The acoustical tensor $\mathbf{Q}(\xi)$ defined in eq. (4) becomes in the new frame

$$\mathbf{Q}(\xi) = (\lambda + c'_{44})\xi \otimes \xi + c'_{44}\xi^2 \mathbf{I} - \frac{1}{3}(\mu_2 - \mu_1) \times$$

$$\begin{bmatrix} \xi_1^2 + \xi_2^2 - 2\sqrt{2}\xi_1\xi_3 & 2\sqrt{2}\xi_2\xi_3 & \sqrt{2}(\xi_2^2 - \xi_1^2) - 2\xi_1\xi_3 \\ 2\sqrt{2}\xi_2\xi_3 & \xi_1^2 + \xi_2^2 + 2\sqrt{2}\xi_1\xi_3 & 2\sqrt{2}\xi_1\xi_2 - 2\xi_2\xi_3 \\ \sqrt{2}(\xi_2^2 - \xi_1^2) - 2\xi_1\xi_3 & 2\sqrt{2}\xi_1\xi_2 - 2\xi_2\xi_3 & 2\xi_3^2 \end{bmatrix}, \quad (9)$$

where ξ is also referred to the basis vectors of eq. (7).

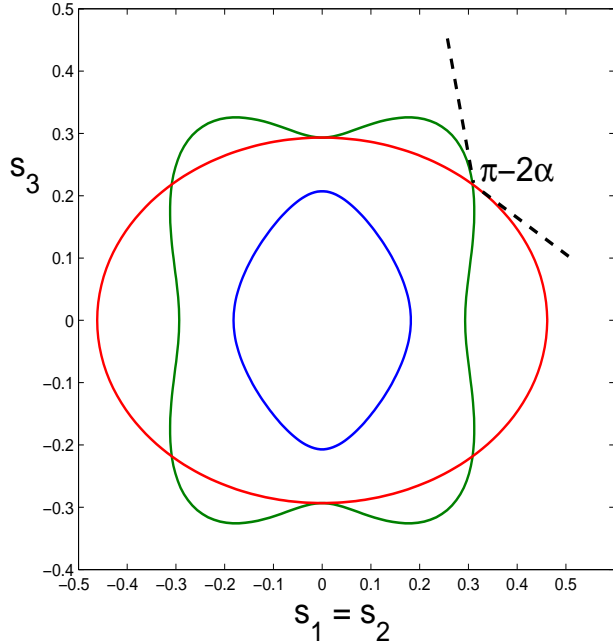


Fig. 2. The section $s_1 = s_2$ of the slowness sheets for Iron, where \mathbf{s} is slowness. The inset depicts the conical section of half angle $\frac{\pi}{2} - \alpha$.

3.2 The slowness surface near the conical point

Although formally exact solutions of the Christoffel equation $\det(\mathbf{Q}(\hat{\xi}) - \rho\mathbf{I}) = 0$ are known for cubic crystals [8], we focus here on an approximation that retains the local geometry near the conical point. The conical point $\xi_0 = \xi_0 \mathbf{e}_3$ is a double root with $\xi_0 = \sqrt{\rho/c'_{44}}$, or

$$\xi_0 = \sqrt{\frac{3\rho}{\mu_1 + 2\mu_2}} \mathbf{e}_3. \quad (10)$$

The slowness surface near the conical point may be approximated locally as an hourglass-type cone, such that

$$\boldsymbol{\xi} = \boldsymbol{\xi}_0 + \zeta \mathbf{e}_3 + \gamma(\zeta, \phi) \mathbf{e}_\phi, \quad (11)$$

where the unit vector \mathbf{e}_ϕ is defined

$$\mathbf{e}_\phi = \cos \phi \mathbf{e}_1 + \sin \phi \mathbf{e}_2. \quad (12)$$

The coordinates ζ and $0 < \phi \leq 2\pi$ will be used to approximate the slowness surface in the vicinity of the conical point $\zeta = 0$.

The approximation used by Burridge [6] was $\gamma = \beta\zeta$, corresponding to a right circular cone, where $\beta = \cot \alpha$, and $\frac{\pi}{2} - \alpha$ is the semi-vertical angle of the right circular tangent cone at the conical point,

$$\tan \alpha = \frac{|c'_{46}|}{c'_{44}} = \sqrt{2} \frac{|\mu_2 - \mu_1|}{\mu_1 + 2\mu_2}. \quad (13)$$

Note that $0 \leq \alpha \leq \arctan \sqrt{2} = 55^\circ$, the lower limit being the isotropic value, and the upper limit occurs as $\mu_2/\mu_1 \rightarrow 0$. The angle $\frac{\pi}{2} - \alpha$ is ν in [6].

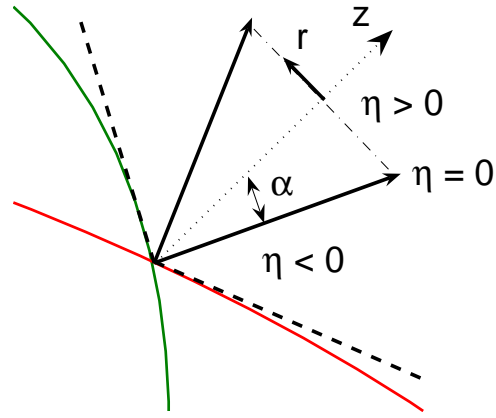


Fig. 3. The conical lid is defined by the cone of semi-angle α in real space. The coordinate z is length along the [111] direction, and r is the perpendicular distance from the axis. The parameter η is the nondimensional distance from the lid edge, eq. (30).

The section of the cone in the plane containing the [110] and [001] axes is shown in Figure 2. The cone in the slowness sheet is defined by the intersection of the quasi-transverse sheets at a point along the [111] direction. The associated wave velocity cone in real space is defined by the normals to the cone, which sweep out a cone of semi-interior angle α in real space. The flat “lid” of this cone is the circular plane lid under investigation. We are particularly interested in the form of the wavefront on the lid and across its boundary edge ($\eta = 0$ in Figure 3). The interior of the lid defines a region in space of solid angle $(1 - \cos \alpha)2\pi$. The eight lids of the slowness surface together define a fraction of total

solid angle equal to $8(1 - \cos \alpha)2\pi/(4\pi) = 4(1 - \cos \alpha)$, which entails as much as 73.4% of space. In other words, the region of influence of the conical point resulting from a point source has influence in, for instance, 37.4% of space in Iron. It is important to realize that the field originates from a single point on the slowness surface, and therefore does not generate energy at infinity. The conical lid wavefront is a nearfield effect.

In order to capture the local curvature of the slowness surface we assume a parabolic approximation to the curvy cone:

$$\gamma(\zeta, \phi) = \beta\zeta + \frac{1}{2}\kappa(\phi)\zeta^2. \quad (14)$$

Substituting from (14) in $\det(\mathbf{Q}(\hat{\boldsymbol{\xi}}) - \rho\mathbf{I}) = 0$ and expanding in powers of ζ , the $O(\zeta^2)$ term implies (13), while the $O(\zeta^3)$ term yields, in agreement with eq. (28) of [15],

$$\begin{aligned} \kappa(\phi) = & \frac{3(\mu_1 + 2\mu_2)^2}{2^{3/2}\xi_0|\mu_2 - \mu_1|^3} \left[\frac{3\mu_1\mu_2}{\mu_1 + 2\mu_2} \right. \\ & \left. - (\mu_2 - \mu_1) \left[1 + \frac{8(\mu_2 - \mu_1)}{9(\lambda + \mu_1)} \right] (1 - (\text{sgn}(\mu_2 - \mu_1)) \cos 3\phi) \right]. \end{aligned} \quad (15)$$

Thus $\kappa(\phi)$ displays three-fold symmetry, with extremal values attained in the directions $\phi = 0$ and $\phi = \pi/3$. The cone angle and curvature for a range of materials are tabulated in Table 1. Note that the curvature for some materials changes signs, indicating that convex and concave sections may coexist. If $\mu_2 - \mu_1 > 0$ define $\kappa_0 = \kappa(0)$, $\kappa_1 = \kappa(\pi/3)$, and if $\mu_2 - \mu_1 < 0$, reverse the definitions. Thus, $\kappa_0 > 0$, and the curvature changes sign iff the ratio κ_1/κ_0 is negative. The vanishing of κ defines a parabolic line, or a line of zero Gaussian curvature. The examples in Figure 1 illustrate the two possibilities: the curvature is always positive for iron but takes both signs for KCl. Parabolic lines have been studied extensively, e.g. [9,15]. Shuvalov and Every [16] provide a detailed study of the shape of the acoustic slowness surface of anisotropic solids near points of conical degeneracy, and show that there can be up to three pairs of lines of zero Gaussian curvature. It may be checked that the condition $\kappa = 0$ is precisely Every's condition F, eq. (16) of [9]. The polarization vector fields near conical points display interesting properties [6,1,2] and we refer the reader to the exhaustive analysis of Shuvalov [14] for details.

3.3 The wave surface

Let the receiver position be defined in the new coordinate system as

$$\mathbf{x} = r\mathbf{e}_\theta + z\mathbf{e}_3, \quad (16)$$

where \mathbf{e}_θ is orthogonal to \mathbf{e}_3 and defined by eq. (12) with ϕ replaced by θ . The contribution to the fundamental solution (2a) from the neighborhood of the conical point follows by approximating the function \mathbf{F} of (2b) locally [6]. As mentioned above, the gradient $\nabla v(\boldsymbol{\xi})$ equals the wave velocity \mathbf{c} , and therefore $|\nabla v(\boldsymbol{\xi})| = c$, the magnitude. The wave velocity

satisfies $\xi \cdot \mathbf{c} = 1$ [12], while near the conical point the approximations $\xi \approx \xi_0$ and $\hat{\xi} \cdot \hat{\mathbf{c}} \approx \cos \alpha$ hold. The first is clear, while the second is a consequence of the fact that the slowness surface is to leading order conical. Hence, $c \approx 1/(\xi_0 \cos \alpha)$. The polarization has the form $\mathbf{A} = \mathbf{e}_{\pi/2-\phi/2}$ (eq. (7.15) of [6]) which together with the approximation for $|\nabla v(\xi)|$ leads to

$$\mathbf{G} \approx -\frac{\xi_0 \cos \alpha}{16\pi^2} \int_{S_c} dS \begin{bmatrix} 1 - \cos \phi & \sin \phi & 0 \\ \sin \phi & 1 + \cos \phi & 0 \\ 0 & 0 & 0 \end{bmatrix} \delta'(t - \xi \cdot \mathbf{x}). \quad (17)$$

Here S_c denotes the slowness surface in the vicinity of the conical point. Also, the matrix elements are referred to the local basis $\{\mathbf{e}_1, \mathbf{e}_2, \mathbf{e}_3\}$. It is important to note that S_c is single-valued and that the two distinct quasi-transverse slownesses are included by virtue of the fact that both $\zeta < 0$ and $\zeta > 0$ must be considered in the integral. This implies that the neighboring sheets at coincident values of $|\zeta|$ correspond to \mathbf{e}_ϕ and $\mathbf{e}_{\phi+\pi}$ and the associated polarizations are (as above) $\mathbf{A} = \mathbf{e}_{\phi/2}$ and $\mathbf{A} = \mathbf{e}_{\phi/2+\pi/2}$, respectively. This formulation obviates the need to distinguish the two almost degenerate sheets. We note that the surface measure is $dS = [(1 + \gamma_\zeta^2)\gamma^2 + \gamma_\phi^2]^{1/2} d\zeta d\phi$, where $\gamma_\zeta \equiv \partial\gamma/\partial\zeta = \beta + \kappa(\phi)\zeta$ and $\gamma_\phi \equiv \partial\gamma/\partial\phi = \frac{1}{2}\kappa'(\phi)\zeta^2$.

The difficulty in evaluating (17) arises from the phase term

$$\xi \cdot \mathbf{x} = \xi_0 z + \zeta z + \gamma(\zeta, \phi) r \cos(\phi - \theta), \quad (18)$$

which follows from (16) and the local approximation (11). As Table 1 demonstrates, the slowness surface curvature parameter κ defined in (14) varies with ϕ , and can change sign.

3.3.1 Local approximation of the wave surface

The wave (or group) velocity vector \mathbf{c} is normal to the slowness surface and satisfies $\mathbf{c} \cdot \xi = 1$. These properties, combined with the slowness in eq. (11) imply

$$\mathbf{c} = (\gamma_\zeta \mathbf{e}_3 - \mathbf{e}_\phi + (\gamma_\phi/\gamma) \mathbf{e}_{\phi+\frac{\pi}{2}}) / [(\xi_0 + \zeta) \gamma_\zeta - \gamma]. \quad (19)$$

In order to derive eq. (19), first note that the partial derivatives of the slowness follow from eqs. (11) and (12) as $\xi_\zeta = \mathbf{e}_3 + \gamma_\zeta \mathbf{e}_\phi$ and $\xi_\phi = \gamma_\phi \mathbf{e}_\phi + \gamma \mathbf{e}_{\phi+\frac{\pi}{2}}$. These are tangent vectors to the slowness surface, and the direction of \mathbf{c} is therefore defined by their cross product. This may be readily evaluated using the orthonormal properties of the triad $\{\mathbf{e}_\phi, \mathbf{e}_{\phi+\frac{\pi}{2}}, \mathbf{e}_3\}$. Then using eq. $\mathbf{c} \cdot \xi = 1$ to fix the magnitude, we arrive at the expression for \mathbf{c} .

Consider a field point in the direction of the wave velocity:

$$\mathbf{x} \equiv z\mathbf{e}_3 + r\mathbf{e}_\perp = t\mathbf{c}, \quad (20)$$

where \mathbf{e}_\perp is the unit vector in the direction of the projection of \mathbf{c} on the plane perpendicular to the \mathbf{e}_3 direction (the [111] axis). It follows from eq. (19) as $\mathbf{e}_\perp = (-\mathbf{e}_\phi + (\gamma_\phi/\gamma)\mathbf{e}_{\phi+\frac{\pi}{2}})/\sqrt{1 + (\gamma_\phi/\gamma)^2}$. Equating components in the directions \mathbf{e}_3 and \mathbf{e}_\perp yields two relations, which we write as

$$t = \xi_0 z + \zeta z - \frac{\gamma r}{\sqrt{1 + (\gamma_\phi/\gamma)^2}}, \quad \frac{z}{r} = \frac{\gamma \zeta}{\sqrt{1 + (\gamma_\phi/\gamma)^2}}. \quad (21)$$

These identities are exact and provide implicit relations between the field point and the location of the point on the slowness surface, characterized by the variables ζ and ϕ in the vicinity of the conical point. In particular, we have not yet invoked the parabolic approximation (14). Use of this allows us to solve for the position on the slowness surface associated with a field position lying near the circular boundary of the lid in physical space. The edge of the lid is defined by

$$z - r\beta = 0, \quad \text{where } \beta = \cot \alpha. \quad (22)$$

Table 1. The cone angle α and the nondimensionalized curvature $\bar{\kappa}(\phi) \equiv \kappa(\phi) \xi_0 / \beta$ follow from equations (13) and (15) and $\beta = \cot \alpha$. Here $\kappa_0 = \kappa(0)$, $\kappa_1 = \kappa(\pi/3)$ if $\mu_2 - \mu_1 > 0$ with the definitions reversed if $\mu_2 - \mu_1 < 0$. Cubic elastic constants from Musgrave [12].

Material	α (deg)	$\bar{\kappa}_0$	κ_1/κ_0
diamond	5.32	122.03	1.33
aluminum	5.41	117.93	1.36
silicon	12.61	22.14	1.70
germanium	14.39	16.94	1.77
silver chloride	14.82	10.61	-0.69
potassium chloride	20.46	4.29	-3.58
iron	25.02	5.11	2.35
nickel	25.38	4.93	2.37
gold	28.56	3.68	2.87
silver	29.59	3.35	2.79
copper	30.95	2.96	2.83
potassium	42.16	1.00	4.23
sodium	44.84	0.72	4.34
β -brass	45.28	0.68	5.10
lithium	53.01	0.10	20.33

The idea is to solve eq. (21)₂ for ζ using (14) with the assumption that $z - r\beta \approx 0$. This amounts to finding solutions to leading order in the small parameter ζ . Thus, we find

$$\zeta = \frac{z - r\beta}{\kappa r} + O((z - r\beta)^2). \quad (23)$$

Substituting into (21) and again expanding in ζ gives

$$t = \xi_0 z + \frac{(z - r\beta)^2}{2\kappa r} + O((z - r\beta)^3). \quad (24)$$

The critical parameter in the previous two results is the curvature $\kappa(\phi)$, which is evaluated at the value of ϕ defined implicitly by eq. (20). The expansion in terms of $(z - r\beta)$ fails if κ vanishes, and clearly a different scaling is necessary near values of ϕ at which $\kappa(\phi) = 0$. We explicitly avoid such directions.

For the remainder of the paper we adopt the major simplification that the curvature κ is independent of ϕ and hence γ is azimuthally symmetric,

$$\gamma = \gamma(\zeta). \quad (25)$$

The removal of the variation in curvature with azimuth leads to tractable expressions for the Green's function, ones that are more detailed than those of Burridge [6], yet which retains the essential physics. At the same time, the approximation is not overly excessive in the sense that we expect all directions of observation will display the same general properties found here. The exceptions are for receiver positions defined by the possible parabolic lines on the slowness surface along which $\kappa(\phi)$ vanishes, which is outside the scope of the present analysis.

4 Evaluation of the Green's function

4.1 Reduction to a single integral

As discussed we restrict attention to the case of κ independent of ϕ . Under this assumption the azimuthal integral in (17) may be effected. First change from ϕ to $\psi = \phi - \theta$, and noting that $dS = |\gamma(\zeta)| \sqrt{1 + \gamma_\zeta^2} d\zeta d\psi$, we obtain

$$\begin{aligned} \mathbf{G} \approx & -\frac{\xi_0 \cos \alpha}{8\pi} \int d\zeta |\gamma(\zeta)| \sqrt{1 + \gamma_\zeta^2} \\ & \times \int \frac{d\psi}{2\pi} \begin{bmatrix} 1 - \cos \theta \cos \psi & \sin \theta \cos \psi & 0 \\ \sin \theta \cos \psi & 1 + \cos \theta \cos \psi & 0 \\ 0 & 0 & 0 \end{bmatrix} \delta'(T - R \cos \psi). \end{aligned} \quad (26)$$

Here,

$$T = t - \xi_0 z - \zeta z, \quad R = \gamma(\zeta) r. \quad (27)$$

The integral can be performed using the identity

$$\int_0^{2\pi} \frac{d\psi}{2\pi} f(\cos \psi) \delta'(T - R \cos \psi) = \frac{1}{\pi R^2} \frac{d}{dx} \left(\frac{f(x)}{\sqrt{1-x^2}} \right) \Big|_{x=T/R} H(R^2 - T^2), \quad (28)$$

where H is the Heaviside step function ($H(t) = 0, \frac{1}{2}, 1$ for $t < 0, = 0, > 0$, respectively) with the result,

$$\mathbf{G} \approx -\frac{\xi_0 \cos \alpha}{8\pi^2} \int d\zeta |\gamma(\zeta)| \sqrt{1+\gamma_\zeta^2} \begin{bmatrix} T - R \cos \theta & R \sin \theta & 0 \\ R \sin \theta & T + R \cos \theta & 0 \\ 0 & 0 & 0 \end{bmatrix} \frac{H(R^2 - T^2)}{(R^2 - T^2)^{3/2}}. \quad (29)$$

Define two new dimensionless parameters

$$\tau = \frac{2\kappa r}{(z + r\beta)^2} (t - \xi_0 z), \quad \eta = \frac{z - r\beta}{z + r\beta}. \quad (30)$$

τ is a reduced time variable relative to the time of arrival of the flat lid wavefront, and η defines distance from the lid edge, with $\eta > 0$ (< 0) if the observer lies inside (outside) the lid, see Figure 3. Let $x = \kappa r \zeta / (z + r\beta)$, then it may be checked that

$$R^2 - T^2 = \frac{(z + r\beta)^4}{(2\kappa r)^2} \left[(x + 1)^2 - (1 + \tau) \right] \left[(x - \eta)^2 - (\eta^2 - \tau) \right]. \quad (31)$$

There are four roots to $R^2 - T^2 = 0$, at $x = \eta \pm (\eta^2 - \tau)^{1/2}$ and $x = -1 \pm (1 + \tau)^{1/2}$. Points near the edge of the lid are characterized by $|\eta| \ll 1$, and the associated wavefronts from the lid and the “regular” wave arrive at times such that the time parameter τ is also small. Of the four roots, all are at values of x that are asymptotically small except the single spurious root at $x = -1 - (1 + \tau)^{1/2} \approx -2$. The origin of this root lies with the parabolic approximation to the sheets of the slowness surface, and it is not a real effect in elasticity. We therefore ignore this root and replace (31) by the cubic approximation

$$R^2 - T^2 = \frac{(z + r\beta)^4}{(2\kappa r)^2} g(x), \quad \text{with} \quad g(x) = (2x - \tau) \left[(x - \eta)^2 - (\eta^2 - \tau) \right]. \quad (32)$$

We make the further approximation $\sqrt{1 + (\gamma_\zeta)^2} \approx \csc \alpha$, which is valid near the conical point. Then noting that

$$\frac{\zeta T}{(R^2 - T^2)^{3/2}} = -\partial_z \frac{1}{(R^2 - T^2)^{1/2}}, \quad (33a)$$

$$\frac{\zeta R}{(R^2 - T^2)^{3/2}} = -\frac{1}{r} \partial_\beta \frac{1}{(R^2 - T^2)^{1/2}} \approx -\frac{1}{\beta} \partial_r \frac{1}{(R^2 - T^2)^{1/2}}, \quad (33b)$$

where ∂_z is $\frac{\partial}{\partial_z}$, etc., we deduce from eqs. (29) through (32) that

$$\mathbf{G} \approx \frac{\beta \xi_0}{8\pi} \begin{bmatrix} \beta \partial_z - \cos \theta \partial_r & \sin \theta \partial_r & 0 \\ \sin \theta \partial_r & \beta \partial_z + \cos \theta \partial_r & 0 \\ 0 & 0 & 0 \end{bmatrix} \frac{I(\tau, \eta)}{z + r\beta}, \quad (34)$$

where I is the integral

$$I(\tau, \eta) = \frac{2}{\pi} \int_{-\infty}^{\infty} dx \operatorname{sgn}(x) \frac{H(g(x))}{\sqrt{g(x)}}. \quad (35)$$

4.2 Evaluation of the integral

The integral (35) can always be reduced to a sum of elliptic integrals, which in turn depend upon the number of roots of $g(x) = 0$. Because $g(x)$ is cubic it can have either one or three real roots. Two distinct cases must be distinguished:

$$\tau < \eta^2, \quad \text{three roots} \quad (36a)$$

$$\tau > \eta^2, \quad \text{one root.} \quad (36b)$$

It is useful to introduce two new parameters,

$$\Delta\tau = \tau - \eta^2, \quad (37)$$

which is the time relative to the curved “regular” wavefront, and

$$\tan \Phi = \frac{\eta - \frac{\tau}{2}}{\sqrt{|\Delta\tau|}}, \quad -\frac{\pi}{2} < \Phi < \frac{\pi}{2}. \quad (38)$$

We examine the two cases (36a) and (36b) separately.

4.2.1 Before the regular front

We consider $\tau < \eta^2$, for which there are three roots to $g(x) = 0$. Denote the roots by $a > b > c$, then it follows from (32) that $abc = \tau^2/2 > 0$. The roots are therefore either all positive, or two are negative and one positive. In either case, (35) becomes

$$I = \frac{\sqrt{2}}{\pi} \left[\operatorname{sgn}(c) \int_c^b \frac{dx}{\sqrt{(x-a)(x-b)(x-c)}} + \int_a^\infty \frac{dx}{\sqrt{(x-a)(x-b)(x-c)}} \right]. \quad (39)$$

Equations (3.131) of [11] imply that the two integrals in (39) are identical in value and hence they cancel if $c < 0$. Simplifying the integrals gives

$$I = \frac{4\sqrt{2}}{\pi} \frac{H(c)}{\sqrt{a-c}} K\left(\sqrt{\frac{b-c}{a-c}}\right), \quad (40)$$

and K is the complete elliptic integral of the first kind,

$$K(k) = \int_0^{\frac{\pi}{2}} \frac{du}{\sqrt{1-k^2 \sin^2 u}}. \quad (41)$$

Referring to (32) we see that $c > 0$ iff both τ and η are positive. Hence, replacing a , b and c by the appropriate roots $\eta + \sqrt{\eta^2 - \tau}$, $\eta - \sqrt{\eta^2 - \tau}$ and $\frac{\tau}{2}$, respectively, yields

$$I(\tau, \eta) = \frac{4\sqrt{2} H(\tau) H(\eta)}{\pi \sqrt{\eta - \frac{\eta^2}{2} - \frac{\Delta\tau}{2} + \sqrt{-\Delta\tau}}} K\left(\sqrt{\tan(\Phi - \frac{\pi}{4})}\right), \quad (42)$$

where $\Delta\tau$ is defined in (37) and Φ in (38).

4.2.2 After the regular front

We now consider the situation when (36b) holds. In this case $g(x) = 0$ has only one root at $x = \tau/2$ and it follows, using equation (3.138.7) of [11], that

$$I = \frac{\sqrt{2}}{\pi} \int_{\frac{\tau}{2}}^{\infty} \frac{dx}{\sqrt{(x - \frac{\tau}{2})[(x - \eta)^2 + (\tau - \eta^2)]}} = \frac{2}{\pi} \sqrt{\frac{2}{p}} K(q), \quad (43)$$

where

$$p = \sqrt{(\eta - \frac{\tau}{2})^2 + (\tau - \eta^2)}, \quad q = \sqrt{\frac{p + \eta - \frac{\tau}{2}}{2p}}. \quad (44)$$

Substituting from (37) and (38) reduces (43) to

$$I(\tau, \eta) = \frac{2\sqrt{2}}{\pi} \left[\Delta\tau + \left(\frac{\Delta\tau}{2} - \eta + \frac{\eta^2}{2} \right)^2 \right]^{-1/4} K\left(\cos\left(\frac{\Phi}{2} - \frac{\pi}{4}\right)\right). \quad (45)$$

4.2.3 Summary of the two cases

Combining (42) and (45) and using (38) provides us with a concise formula for $I(\tau, \eta)$:

$$I = \frac{2\sqrt{2}}{\pi} \frac{\sqrt{\cos \Phi}}{|\Delta\tau|^{1/4}} \times \begin{cases} \sqrt{2\sqrt{2} \sec(\Phi - \frac{\pi}{4})} K\left(\sqrt{\tan(\Phi - \frac{\pi}{4})}\right) H(\tau) H(\eta), & \Delta\tau < 0, \\ K\left(\cos\left(\frac{\Phi}{2} - \frac{\pi}{4}\right)\right), & \Delta\tau > 0. \end{cases} \quad (46)$$

We are now in a position to apply these formulae and summarize the behavior of the Green's function.

5 Discussion of the wavefront singularities

The contribution to the Green's function from the neighborhood of the conical point is evidently contained in the functional form of eq. (46). In addition to the flat lid response this should include the regular wavefronts associated with the curved surfaces of the two sheets near their point of intersection.

5.1 The flat lid wavefront

The first thing we note is the step discontinuity in I at $\tau = 0$ for $\eta > 0$, i.e., inside the lid, see Figure 3. Using (46) for $\Delta\tau < 0$ and noting that $\Phi = \pi/4$ in this limit, implies

$$I(0+, \eta) - I(0-, \eta) = \frac{2}{\sqrt{\eta}}. \quad (47)$$

Combined with (30) and (34) this gives the contribution to the Green's function from the flat lid,

$$\mathbf{G} \approx \frac{\xi_0 \beta^2}{4\pi} \frac{H(t - \xi_0 z)}{(z^2 - r^2 \beta^2)^{3/2}} \begin{bmatrix} -z & -r\beta \cos \theta & r\beta \sin \theta & 0 \\ & r\beta \sin \theta & -z + r\beta \cos \theta & 0 \\ 0 & & 0 & 0 \end{bmatrix}, \quad \eta > 0. \quad (48)$$

This agrees with equation (7.22) of [6].

5.2 The curved wavefronts near the lid edge

We next consider the singularities at $\Delta\tau = 0$ for $\eta < 0$ and $\eta > 0$, but such that $|\eta| \ll 1$. The latter implies that the field point lies close to the direction $z = r \cot \alpha$, the edge of the lid.

For small η , we have

$$\partial_z \approx \frac{1}{2z} \partial_\eta, \quad \partial_r \approx -\frac{\beta}{2z} \partial_\eta, \quad (49)$$

and therefore from (34),

$$\mathbf{G} \approx \frac{1}{16\pi} \frac{\xi_0}{r^2} \mathbf{A} \mathbf{A}^T \frac{\partial I}{\partial \eta}, \quad (50)$$

where the unit vector \mathbf{A} is now $\mathbf{e}_{-\theta/2}$,

$$\mathbf{A} = \cos \frac{\theta}{2} \mathbf{e}_1 - \sin \frac{\theta}{2} \mathbf{e}_2. \quad (51)$$

The behavior of I as $\Delta\tau \rightarrow 0\pm$ depends upon how Φ of eq. (38) behaves in this limit. We note that

$$\lim_{\Delta\tau \rightarrow 0\pm} \Phi = \frac{\pi}{2} \operatorname{sgn} \eta. \quad (52)$$

The two cases of the observer lying just outside or just inside the lid are considered in sequence.

5.2.1 The convex wavefront outside the lid

First, if $\eta < 0$, it follows from (45), (46) and (52) that

$$I \approx \sqrt{\frac{2}{|\eta|}} H(\Delta\tau), \quad \frac{\partial I}{\partial \eta} \approx 2\sqrt{2|\eta|} \delta(\tau - \eta^2). \quad (53)$$

The behavior of the Green's function near to but outside of the lid edge is therefore, using (30), (50) and (53),

$$\mathbf{G} \approx \frac{\xi_0 \beta^2}{4\pi} \mathbf{A} \mathbf{A}^T \frac{\sqrt{2|\eta|}}{\kappa r} \delta \left(t - \xi_0 z - \frac{(z - r\beta)^2}{2\kappa r} \right), \quad \eta < 0. \quad (54)$$

The delta function singularity is what one would expect from the locally convex shape of the slowness surface and the fact that $\kappa > 0$ is assumed, as occurs, for instance, for iron in Figure 1. Equation (54) also agrees with the general result of eq. (6.8) of [6]. It is interesting to note that the strength of the singularity decreases as $\sqrt{|\eta|}$ as the field point approaches the lid edge.

5.2.2 The saddle-shaped wavefront inside the lid

We next consider the singularity at $\Delta\tau = 0$ for $\eta > 0$, for which we use

$$K(q) \approx \ln \frac{1}{\sqrt{1 - q^2}}, \quad q \rightarrow 1. \quad (55)$$

Equations (42) and (52) together imply that for fixed but asymptotically small and positive η and $\Delta\tau = o(\eta)$,

$$I \approx \frac{2}{\pi} \frac{1}{\sqrt{2\eta}} \ln \frac{1}{|\Delta\tau|}, \quad \Delta\tau \rightarrow 0\pm. \quad (56)$$

Hence,

$$\frac{\partial I}{\partial \eta} \approx -\frac{2}{\pi} \frac{\sqrt{2\eta}}{\Delta\tau + i0}, \quad (57)$$

and the Green's function is

$$\mathbf{G} \approx \frac{\xi_0 \beta^2}{4\pi} \mathbf{A} \mathbf{A}^T \frac{\sqrt{2\eta}}{\kappa r} \frac{1}{\pi \left(t - \xi_0 z - \frac{(z - r\beta)^2}{2\kappa r} + i0 \right)}, \quad \eta > 0. \quad (58)$$

Again, this has the expected form for a singularity associated with a part of the slowness surface which is saddle shaped, in agreement with equation (6.9) of [6]. We note that the magnitude of the singularity also depends upon $\sqrt{\eta}$.

The difference between this case and the prior result eq. (54) is that the the normal to the slowness surface in the latter case is exterior to the cone, while for the present situation it lies inside the conical surface. With reference to the picture for iron in Figure 1, the convex wavefront arises from the lower convex part, while eq. (58) is associated with the interior of the conical "bowl".

5.2.3 Summary of the response inside and outside the lid

The three singularities associated with the lid wavefront and the wavefronts from the convex and saddle-shaped regions near the conical point are described by equations (48), (54) and (58), respectively. In summary, from (54) and (58):

$$\mathbf{G} \approx \frac{\xi_0 \beta^2}{4\pi} \mathbf{A} \mathbf{A}^T \frac{\sqrt{2|\eta|}}{\kappa r} \times \begin{cases} \delta \left(t - \xi_0 z - \frac{(z-r\beta)^2}{2\kappa r} \right), & \eta < 0, \\ \pi^{-1} \left(t - \xi_0 z - \frac{(z-r\beta)^2}{2\kappa r} + i0 \right)^{-1}, & \eta > 0. \end{cases} \quad (59)$$

These results are, so far, predictable from the analysis in [6], combined with the parabolic form of the slowness surface assumed here. In that sense we have not yet derived any new forms of the Green's function, other than to specialize them to the parabolic local approximation of the slowness surface. The remainder of the paper generates expressions that are not special cases of prior results. We conclude this section by considering the field right on the lid edge. The transition from one regime to another is encapsulated in the general expressions of equations (46) and (50) and is examined next. In section 6 we derive uniformly asymptotic expressions that are valid across the lid edge.

5.3 The singularity in the direction of the lid edge

The lid edge direction $z = r \cot \alpha$ is particularly interesting, and the singularity there corresponds to the origin of the nondimensional coordinates: $\eta = \tau = 0$. The general expressions in (46) may be used. In this limit the domain of the term for $\Delta\tau$ vanishes, implying zero field for $\tau < 0$. The field after $\tau = 0$ follows from (46) and (50). Using (38) it is straightforward to show that

$$\left. \frac{\partial I}{\partial \eta} \right|_{\eta=0} = \frac{H(\tau)}{\pi \left(\tau + \frac{\tau^2}{4} \right)^{1/4}} \left[\frac{1}{\sqrt{\tau}} \frac{dK}{dk} \left(\frac{1}{\sqrt{2}} \right) + \frac{1}{\sqrt{2} \left(1 + \frac{\tau}{4} \right)} K \left(\frac{1}{\sqrt{2}} \right) \right]. \quad (60)$$

The derivative of the elliptic integral in (60) simplifies to $\pi/\sqrt{2}K$ for the particular argument $1/\sqrt{2}$ (see eqs. (8.123.2) and (8.122) in [11]). Then using the identity $K(1/\sqrt{2}) =$

$\Gamma^2(1/4)/4\sqrt{\pi}$ from (8.129.1) of [11], where $\Gamma(1/4) \approx 3.62561$, and making the replacement $1 + \tau/4 \rightarrow 1$ in (60), we obtain

$$\frac{\partial I}{\partial \eta} \Big|_{\eta=0} \approx \frac{H(\tau)}{\tau^{3/4}} \frac{2\sqrt{2\pi}}{\Gamma^2(1/4)} \left[1 + \frac{\Gamma^4(1/4)}{16\pi^2} \sqrt{\tau} \right]. \quad (61)$$

The Green's function is therefore, from (50),

$$\mathbf{G} \approx \frac{\xi_0 \beta^2}{4\pi} \mathbf{A} \mathbf{A}^T \sqrt{\frac{\pi}{\beta}} \frac{(2\kappa)^{1/4}}{\Gamma^2(1/4)} \frac{H(t - \xi_0 z)}{\kappa r [r(t - \xi_0 z)^3]^{1/4}} \left[1 + \frac{\Gamma^4(1/4)}{16\pi^2} \left(\frac{\kappa(t - \xi_0 z)}{2\beta z} \right)^{1/2} \right], \quad \eta = 0. \quad (62)$$

6 A uniform solution in rescaled variables

The various singularities and their interaction can be understood by a rescaling suitable for the neighborhood of the lid edge. Let

$$\tau = s \eta^2, \quad (63)$$

where the time-like parameter is

$$s = 2\kappa r \frac{(t - \xi_0 z)}{(z - r\beta)^2}. \quad (64)$$

We recast the results in terms of s and η , where the region of interest is near the lid edge, i.e., $|\eta| \ll 1$ but $s = O(1)$. The three wavefronts discussed in the previous section, the flat lid wavefront, and the “regular” wavefronts inside and outside the cone $z - \beta r = 0$ correspond to $(s = 0, \eta > 0)$, $(s = 1, \eta > 0)$ and $(s = 1, \eta < 0)$, respectively. The rescaled time allows us to separate the three, and to observe their coalescence.

Since $|\eta| \ll 1$, (38) implies that $\tan \Phi \approx \operatorname{sgn} \eta / \sqrt{|s - 1|}$, and after some simplification, (46) reduces to

$$I(\tau, \eta) \approx \frac{2}{\sqrt{|\eta|}} J(s, \operatorname{sgn} \eta), \quad (65)$$

where

$$J(s, \operatorname{sgn} \eta) = \frac{\sqrt{2}}{\pi} \times \begin{cases} 0, & s < 0, \\ 2 \left(1 + \sqrt{1-s} \right)^{-1/2} K \left(\frac{\sqrt{s}}{1+\sqrt{1-s}} \right) H(\operatorname{sgn} \eta), & 0 < s < 1, \\ s^{-1/4} K \left(\sqrt{\frac{1}{2} + \frac{\operatorname{sgn} \eta}{2\sqrt{s}}} \right), & s > 1. \end{cases} \quad (66)$$

Note that J only depends on η via its sign. It follows that

$$\frac{\partial I}{\partial \eta} \rightarrow \frac{-\operatorname{sgn} \eta}{|\eta|^{3/2}} \left[J + 4s \frac{\partial J}{\partial s} \right], \quad \text{for } \eta \neq 0, \quad (67)$$

and so the fundamental solution in the vicinity of the cone $z = r \cot \alpha$ (although not on it, i.e. $\eta \neq 0$) may be written, from (50) and (67), as

$$\mathbf{G} \approx -\frac{\xi_0 \beta^2}{4\pi} \mathbf{A} \mathbf{A}^T 2z \frac{\operatorname{sgn}(z - r\beta)}{|z^2 - r^2 \beta^2|^{3/2}} \left[J(s, \eta) + 4s \frac{\partial J}{\partial s}(s, \eta) \right]. \quad (68)$$

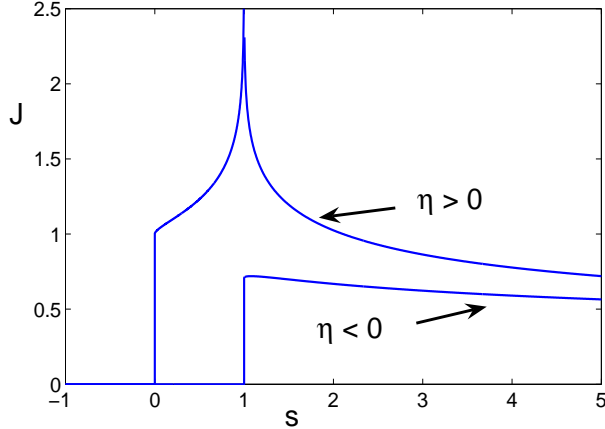


Fig. 4. The function $J(s, \operatorname{sgn} \eta)$ of eq. (66)

The function J is plotted in Figure 4. Note the step singularity at $s = 0$ for $\eta > 0$, corresponding to the lid wavefront of (48). The singularities at $s = 1$ are a step for $\eta < 0$, which results in the delta pulse of (54), and a logarithmic singularity for $\eta > 0$, corresponding to the $1/t$ wave in (58).

The propagating singularities are all contained in the expression $(J + 4s\partial J/\partial s)$ in (68). Because this can exhibit delta function behavior which is difficult to display on a plot, we look instead at the response from a step load, i.e., the solution to (1a) with $\delta(t)$ replaced with $H(t)$. Integrating (68) gives the step response near the edge of the lid as

$$\mathbf{G} \approx \frac{\xi_0 \beta^2}{4\pi} \mathbf{A} \mathbf{A}^T \frac{\sqrt{|\eta|}}{2\kappa r} M(s, \operatorname{sgn} \eta), \quad (69)$$

where

$$\begin{aligned} M(s, \operatorname{sgn} \eta) &= -\operatorname{sgn} \eta \int_0^s \left(J + 4s \frac{\partial J}{\partial s} \right) \mathrm{d} s \\ &= \operatorname{sgn} \eta \left(3 \int_0^s J \mathrm{d} s - 4s J \right). \end{aligned} \quad (70)$$

The function M is plotted in Figure 5. For observers outside the cone, i.e. $z - r\beta < 0$, there is no signal until the arrival of the regular wavefront at $s = 1$ ($\tau = \eta^2$), and is the

step function instead of the delta response in eq. (59). Inside the cone ($z - r\beta > 0$) the first, weak, signal is from the lid edge at $s = 0$ ($\tau = 0$) which has the form of a ramp function, as compared with the step in eq. (48). This is followed by the regular wavefront at $s = 1$ ($\tau = \eta^2$) with a logarithmic singularity.

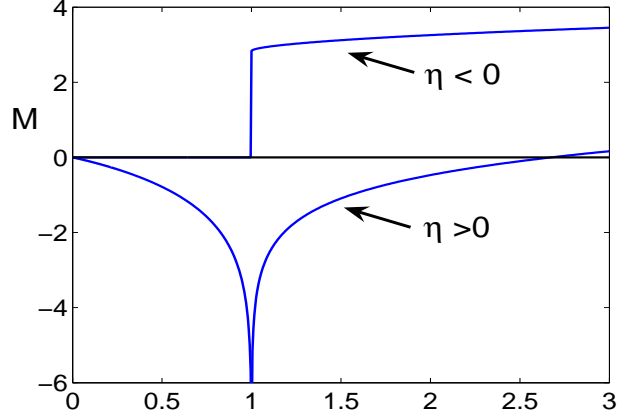


Fig. 5. The function $M(s, \operatorname{sgn} \eta)$ of eq. (70)

The one remaining feature not evident in the uniform solution in terms of the J and M functions is the behavior right on the lid edge. This follows by taking the limit $s \rightarrow \infty$ with $\eta \neq 0$. Using (66) and integrating by parts, gives

$$\begin{aligned} M(s, \operatorname{sgn} \eta) - M(1, \operatorname{sgn} \eta) &= \frac{1}{\pi} \int_1^s \frac{ds}{s^{3/4}} \frac{1}{\sqrt{1 + \frac{\operatorname{sgn} \eta}{\sqrt{s}}}} \frac{dK}{dk} \left(\sqrt{\frac{1}{2} + \frac{\operatorname{sgn} \eta}{2\sqrt{s}}} \right) \\ &= \frac{8\sqrt{2\pi}}{\Gamma^2(1/4)} s^{1/4} + O(1), \quad s \rightarrow \infty. \end{aligned} \quad (71)$$

Thus $M(s, \operatorname{sgn} \eta)$ becomes independent of $\operatorname{sgn} \eta$ for large s , and grows as $1.5255 s^{1/4}$, which is consistent with the $1/t^{3/4}$ singularity along the directions for which $\eta = 0$, see equation (62).

7 Conclusion

We have revisited the problem of determining the waves emanating from the vicinity of the conical point in materials with cubic symmetry. The analysis is based on the general formulation of Burridge [6] and employs a higher order approximation to the slowness surface. The key ingredient is the parabolic approximation (14) for the vicinity of the conical point, which depends upon the curvature κ of eq. (15). By assuming the curvature is constant in the azimuth the evaluation of the Green's function is reduced to a single integral (35). This reproduces the flat lid singularity (48) derived by Burridge [6] as well as the regular wavefronts originating near the conical point. The wavefront singularity on the lid edge, eq. (62), has been evaluated. A uniformly valid representation is presented for the transition as the observation direction crosses the lid edge. This involves a single

function, based on rescaled space and time coordinates, that displays the regular wavefront singularities and the flat lid singularity.

Acknowledgment

Helpful suggestions from A. L. Shuvalov are appreciated.

References

- [1] V. I. Al'shits and J. Lothe, *Elastic waves in triclinic crystals. I. General theory and the degeneracy problem*, Sov. Phys. Crystallogr. **24** (1979), 387–392.
- [2] ———, *Elastic waves in triclinic crystals. II. Topology of polarization fields and some general theorems*, Sov. Phys. Crystallogr. **24** (1979), 393–398.
- [3] B. A. Auld, *Acoustic Fields and Waves in Solids*, vol. 1, Wiley Interscience, New York, 1973.
- [4] P. A. Barry and M. J. P. Musgrave, *On elliptical conical refraction of elastic waves in tetragonal media*, Q. J. Mech. Appl. Math. **32** (1979), 205–214.
- [5] V. A. Borovikov, *The stationary phase method for surfaces with conical points*, Russian J. Math. Phys. **7** (2000), 147–165.
- [6] R. Burridge, *The singularity on the plane lids of the wave surface of elastic media with cubic symmetry*, Q. J. Mech. Appl. Math. **20** (1967), 41–56.
- [7] R. Courant and D. Hilbert, *Methods of Mathematical Physics*, vol. 2, Interscience, New York, 1962.
- [8] A. G. Every, *General closed-form expressions for acoustic waves in cubic crystals*, Phys. Rev. Lett. **42** (1979), 1065–1068.
- [9] ———, *Ballistic phonons and the shape of the ray surface in cubic crystals*, Phys. Rev. B **24** (1981), 3456–3467.
- [10] A. G. Every and K. Y. Kim, *Time domain dynamic response functions of elastically anisotropic solids*, J. Acoust. Soc. Am. **95** (1994), 2505–2516.
- [11] I. S. Gradshteyn, I. M. Ryzhik, A. Jeffrey, and D. Zwillinger, *Table of Integrals, Series, and Products*, Academic Press: San Diego, CA, 2000.
- [12] M. J. P. Musgrave, *Crystal Acoustics*, Acoustical Society of America, New York, 2003.
- [13] R. G. Payton, *Wave propagation in a restricted transversely isotropic solid whose slowness surface contains conical points*, Q. J. Mech. Appl. Math. **45** (1992), 183–197.
- [14] A. L. Shuvalov, *Topological features of the polarization fields of plane acoustic waves in anisotropic media*, Proc. R. Soc. A **454** (1998), 2911–2947.

- [15] A. V. Shuvalov and A. G. Every, *Curvature of acoustic slowness surface of anisotropic solids near symmetry axes*, Phys. Rev. B **53** (1996), 14906–14916.
- [16] ———, *Shape of the acoustic slowness surface of anisotropic solids near points of conical degeneracy*, J. Acoust. Soc. Am. **101** (1997).